Inorg. Chem. **2006**, *45*, 2229–2234

Design of a Magnetic Bistability Molecular System Constructed by H-Bonding and $\pi\cdots\pi$-Stacking Interactions

X. M. Ren,*[,†,‡] S. Nishihara,[§] T. Akutagawa,[†,‡] S. Noro,[†,‡] and T. Nakamura*[,†,‡]

Research Institute for Electronic Science, Hokkaido University, Sapporo 060-0812, Japan, and CREST, Japan Science and Technology Corporation (JST), Kawaguchi 332-0012, Japan, and Department of Chemistry, Graduate School of Science, Nagoya University, Chikusa-ku, Nagoya 464-8602, Japan

Received September 12, 2005

Crystal structures and magnetic properties were determined for two novel polymorphs of the complex $[H_2DABCO][Ni(mnt)_2]$ [$(H_2DABCO)^{2+}$ = diprotonated 1,4-diazabicyclo[2.2.2]octane; mnt^{2-} = maleonitriledithiolate]. For each polymorph, anions form a layered structure in which two kinds of dimers were observed. The adjacent anionic sheets are held together by cations via H-bonding interactions between protons of cations and CN groups of anions. Two polymorphs possess spin bistability; namely, upon cooling, a magnetic transition happens at around 120 K with about 1 K hysteresis on heating for the α phase and at 112 K with about 10 K hysteresis for the β phase. Above the transition, the magnetic behaviors of two polymorphs can be approximately interpreted by a singlet–triplet model of an antiferromagnetically coupled $S = {}^1/_2$ dimer, which is supported by the crystal structures and spin dimer analyses based on extended Hückel molecular orbital calculations.

Introduction

Crystal engineering permits the rational design of functional molecular materials that exhibit technologically useful physical properties. For instance, a molecular material with electron and cation mixed transport was created by combining a crown-ether-based ionic channel of a supramolecular system and the architecture of a molecular conductor.[1] A multifunctional molecular material with coexistence of ferromagnetism and metallic conductivity was obtained by inserting the building blocks of a molecular conductor into molecular ferromagnetic layers.[2] The study of utilizing crystal-oriented syntheses via noncovalent interactions, such as H-bonding and $\pi-\pi$ stacking interactions between suitable molecules or ions to generate functional materials, has attracted considerable attention.[3−7]

We are interested in developing a new spin-transition molecular system that may have potential applications in molecular spin-electronic or "spintronic" devices, such as molecular switches, data storage devices, and displays.[4,8−12] Molecules that possess a planar structure with an extended electronic structure (for example, $[M(mnt)_2]^-$,[13] TTF^+,[14] and its derivatives, $TCNQ^-$ and $TCNE^-$,[15] 1,3,5-trithia-2,4,6-

* To whom correspondence should be addressed. E-mail: xmren@es.hokudai.ac.jp (X.M.R.), tnaka@imd.es.hokudai.ac.jp (T.N.). Tel: +81 11-706-2849. Fax: +81 11-706-4972.

† Hokkaido University.

‡ JST.

§ Nagoya University.

(1) Nakamura, T.; Akutagawa, T.; Honda, K.; Underhill, A. E.; Coomber, A. T.; Friend, R. H. *Nature* **1998**, *394*, 159.

(2) Coronado, E.; Galén-Mascarós, J. R.; Gómez-Garcia, C. J.; Laukhin, V. *Nature* **2000**, *408*, 447.

(3) Braga, D.; Maini, L.; Polito, M.; Grepioni, F. *Struct. Bonding* **2004**, *111*, 1.

(4) (a) Miller, J. S. *Angew. Chem., Int. Ed.* **2003**, *42*, 27. (b) Itkis, M. E.; Chi, X.; Cordes, A. W.; Haddon, R. C. *Science* **2002**, *296*, 1443.

(5) Ren, X. M.; Chen, Y. C.; He, C.; Gao, S. *J. Chem. Soc., Dalton Trans.* **2002**, 3915.

(6) Paraschiv, C.; Ferlay, S.; Hosseini, M. W.; Bulach, V.; Planeix, J.-M. *Chem. Commun.* **2004**, 2270.

(7) Akutagawa, T.; Takeda, S.; Hasegawa, T.; Nakamura, T. *J. Am. Chem. Soc.* **2004**, *126*, 291.

(8) (a) Fujita, W.; Awaga, K. *Science* **1999**, *286*, 261. (b) Brusso, J. L.; Clements, O. P.; Haddon, R. C.; Itkis, M. E.; Leitch, A. A.; Oakley, R. T.; Reed, R. W.; Richardson, J. F. *J. Am. Chem. Soc.* **2004**, *126*, 8256.

(9) Kahn, O.; Martinez, C. J. *Science* **1998**, *279*, 44.

(10) Gutlich, P.; Garcia, Y.; Woike, T. *Coord. Chem. Rev.* **2001**, *219*, 839.

(11) (a) Kosaka, W.; Nomura, K.; Hashimoto, K.; Ohkoshi, S. *J. Am. Chem. Soc.* **2005**, *127*, 8590. (b) Galet, A.; Niel, V.; Munõz, M. C.; Real, J. A. *J. Am. Chem. Soc.* **2003**, *125*, 14224. (c) Migliori, J. M.; Reiff, W. M.; Arif, A. M.; Miller, J. S. *Inorg. Chem.* **2004**, *43*, 6875. (d) Bousseksou, A.; Molnar, G.; Matouzenko, G. *Eur. J. Inorg. Chem.* **2004**, *22*, 4353.

(12) Letard, J. F.; Guionneau, P.; Goux-Capes, L. *Top. Curr. Chem.* **2004**, *235*, 221 and references cited therein.

(13) (a) Pullen, A. E.; Faulmann, C.; Pokhodnya, K. I.; Cassoux, P.; Tokumoto, M. *Inorg. Chem.* **1998**, *37*, 6714. (b) Coomber, A. T.; Beljonne, D.; Friend, R. H.; Brédas, J. L.; Charlton, A.; Robertson, N.; Underhill, A. E.; Kurmoo, M.; Day, P. *Nature* **1996**, *380*, 144.

10.1021/ic051563k CCC: $33.50
Published on Web 02/02/2006

Table 1. Crystallographic Data for the α and β Phases of **1**

	α(293 K)	α(100 K)	β(293K)	β(100K)
molecular formula	$C_{22}H_{14}N_{10}S_8Ni_2$	$C_{22}H_{14}N_{10}S_8Ni_2$	$C_{22}H_{14}N_{10}S_8Ni_2$	$C_{22}H_{14}N_{10}S_8Ni_2$
CCDC no.	CCDC 265352	CCDC 265353	CCDC 265354	CCDC 265355
molecular mass	792.33	792.33	792.33	792.33
space group	$P\bar{1}$	$P\bar{1}$	$P\bar{1}$	$P\bar{1}$
a/Å	10.009(2)	9.972(5)	6.4778(13)	6.3719(13)
b/Å	10.247(2)	10.022(4)	14.959(3)	15.013(3)
c/Å	15.618(3)	15.416(8)	15.262(3)	15.016(3)
α/deg	76.25(3)	70.825(15)	89.60(3)	89.88(3)
β/deg	71.59(3)	78.295(18)	81.07(3)	82.23(3)
γ/deg	87.36(3)	87.343(17)	82.61(3)	82.44(3)
V/Å^3	1475.4(5)	1424.6(12)	1448.7(5)	1410.7(5)
Z	2	2	2	2
μ/mm^{-1}	1.878	1.945	1.913	1.964
λ/Å	0.71073	0.71073	0.71073	0.71073
ρ/(g·cm^{-3})	1.783	1.847	1.816	1.865
GOF on F^2	1.108	1.062	1.056	1.018
R1, wR2 [$I > 2\sigma(I)$][a]	0.0336, 0.0830	0.0447, 0.1299	0.0245, 0.0574	0.0262, 0.0900
R1, wR2 (all data)[a]	0.0557, 0.1189	0.0574, 0.1675	0.0352, 0.0780	0.0262, 0.0900
largest diff peak and hole (e·Å^{-3})	0.586,−0.673	0.829,−1.357	0.357, −0.348	0.0325, 0.1197

[a] $R1 = \sum(||F_o| - |F_c||)/\sum|F_o|$; $wR2 = \sum w(|F_o|^2 - |F_c|^2)^2/\sum w(|F_o|^2)^2]^{1/2}$.

triazapentalenyl radical (TTTA),[8] and so on) are favorable in forming stacks via intermolecular $\pi-\pi$ interactions. Both the spin-polarization and orbital overlap dominate the magnetic-exchange interactions within a stack. Accordingly, the magnetic-exchange behavior is sensitive to the intermolecular contacts and overlap patterns. For such a molecular system, external perturbations, such as a change of temperature or application of pressure, that affect intermolecular contacts and overlapping patterns may trigger a spin transition. Our studies have focused on the design, preparation, and investigation of a novel spin-transition system based on the molecular architecture of a $[M(mnt)_2]^-$ monoanion (mnt^{2-} = maleonitriledithiolate; M = Ni, Pd, or Pt). Benzylpyridinium derivatives ($[RBzPy]^+$) were employed as the countercation of $[M(mnt)_2]^-$ ions to prepare a series of compounds with a spin transition.[16] For each of the complexes, the transition is very sharp, but hysteresis was not observed. It is important to note that hysteresis, which makes two states stable, is essential for many applications.[12] It was noted that intermolecular cooperativity plays an important role in widening hysteresis in transition-metal spin-crossover systems and the TTTA radical system.[8,9,12] This provides the motivation to introduce a countercation that is a potential H-bonding donor to the spin system of $[M(mnt)_2]^-$. The group of CN in the ligand of mnt^{2-} can act as an H-bonding acceptor,[5,17] so that the intermolecular cooperativity in the spin system of $[M(mnt)_2]^-$ is strengthened and perhaps a spin-transition system with hysteresis can be developed.

Herein, we present two polymorphs (each one is referred to the α and β phases) of a compound $[H_2DABCO][Ni(mnt)_2]_2$ (**1**; $[H_2DABCO]^{2+}$ = diprotonated 1,4-diazabicyclo[2.2.2]octane), each of which displays a spin transition with a clear hysteresis loop.

Experimental Section

$[H_2DABCO][Ni(mnt)_2]_2$ (**1**) was prepared according to the method in the literature.[16] Elem anal. Calcd for $C_{22}H_{14}N_{10}S_8Ni_2$: C, 33.3; H, 1.78; N, 17.7. Found: C, 33.1; H, 1.79; N, 17.5. The single crystals of the α phase were obtained by evaporating a MeCN solution of **1**, while the crystals of the β phase were obtained by dispersing Et_2O into a MeCN solution of **1**.

Magnetic susceptibility measurements for a polycrystalline sample were carried out by a Quantum Design MPMS-XL superconducting quantum interference device (SQUID) magnetometer in the range of 2−350 K.

Crystallographic data were collected using a Rigaku RAXIS−RAPID diffractometer with Mo Kα (λ = 0.710 73 Å) radiation from a graphite monochromator. Structures were solved by direct methods using the *SHELXL-97* software package,[18] and refinements were performed using the full-matrix least-squares method on F^2. Parameters were refined anisotropically, with the exception of those for hydrogen atoms. All H atoms were placed at calculated positions (C−H = 0.930 Å for benzene or pyridine rings and 0.970 Å for methylene) and refined by riding on the parent atoms with $U(H) = 1.2U_{eq}$ (bonded C atom). Crystallographic data were summarized in Table 1.

Results and Discussion

Figure 1 shows the ORTEP view of the α phase at 293 K. An asymmetric unit contains two crystallographically

(14) Ward, B. H.; Granroth, G. E.; Abboud, K. A.; Meisel, M. W.; Talham, D. R. *Chem. Mater.* **1998**, *10*, 1102.

(15) Ballester, L.; Gutiérrez, A.; Perpiñán, M. F.; Rico, S.; Azcondo, M. T.; Bellitto, C. *Inorg. Chem.* **1999**, *38*, 4430.

(16) (a) Ren, X. M.; Meng, Q. J.; Song, Y.; Lu, C. S.; Hu, C. J.; Chen, X. Y. *Inorg. Chem.* **2002**, *41*, 5686. (b) Xie, J. L.; Ren, X. M.; Song, Y.; Zheng, W. W.; Liu, W. L.; He, C.; Meng, Q. J. *Chem. Commun.* **2002**, 2346. (c) Xie, J. L.; Ren, X. M.; He, C.; Gao, Z. M.; Song, Y.; Meng, Q. J.; Kremer, R. K. *Chem. Phys. Lett.* **2003**, *369*, 41. (d) Ren, X. M.; Okudera, H.; Kremer, R. K.; Song, Y.; He, C.; Meng Q. J.; Wu, P. H. *Inorg. Chem.* **2004**, *43*, 2569. (e) Ni, C. L.; Dang, D. B.; Song, Y.; Gao, S.; Li, Y. Z.; Ni, Z. P.; Tian, Z. F.; Wen, L. L.; Meng, Q. J. *Chem. Phys. Lett.* **2004**, *396*, 353. (f) Ni, C. L.; Dang, D. B.; Li, Y. Z.; Yuan, Z. R.; Ni, Z. P.; Tian, Z. F.; Meng, Q. J. *Inorg. Chem. Commun.* **2004**, *7*, 1034. (g) Ni, C. L.; Li, Y. Z.; Dang, D. B.; Ni, Z. P.; Tian, Z. F.; Yuan, Z. R.; Meng, Q. J. *Inorg. Chem. Commun.* **2005**, *8*, 105. (h) Ni, C. N.; Dang, D. B.; Li, Y. Z.; Gao, S.; Ni, Z. P.; Tian, Z. F.; Meng, Q. J. *J. Solid State Chem.* **2005**, *178*, 100. (i) Dang, D. B.; Ni, C. L.; Bai, Y.; Tian, Z. F.; Ni, Z. P.; Wen, L. L.; Meng, Q. J.; Gao, S. *Chem. Lett.* **2005**, *34*, 680. (j) Ren, X. M.; Akutagawa, T.; Nishihara, S.; Nakamura, T.; Fujita, W.; Awaga, K. *J. Phys. Chem. B* **2005**, *109*, 16610.

(17) Crawford, P. C.; Gillon, A. L.; Green, J.; Orpen, A. G.; Podesta, T. J.; Pritchard, S. V. *CrystEngComm* **2004**, *6*, 419.

(18) Sheldrick, G. M. *SHELXTL-97, Structure Determination Software programs*, version 5.10; Bruker Analytical X-ray Systems Inc.: Madison, WI, 1997.

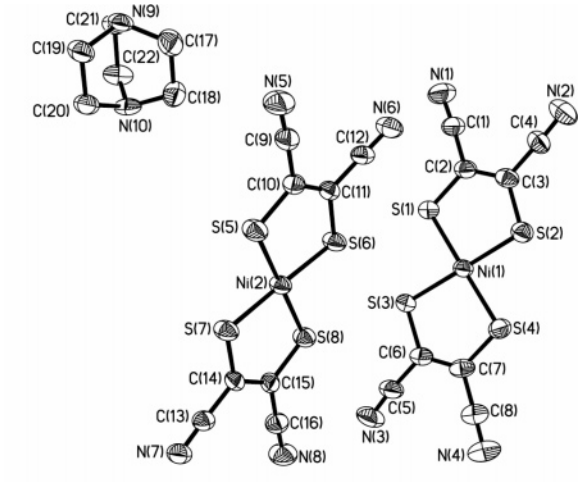

Figure 1. ORTEP view of the α phase (with the displacement ellipsoids at the 50% probability level and H atoms omitted for clarity) at 293 K.

independent $[Ni(mnt)_2]^-$ units and one $[H_2DABCO]^{2+}$ cation. The bond lengths in the two anionic molecules are very close to each other and are in good agreement with those values in other $[Ni(mnt)_2]^-$ compounds.[16] The core of NiS_4 is slightly distorted from a square-planar geometry in each crystallographically independent anion. Two anionic mean planes, defined by the core of NiS_4, make a dihedral angle of 70.3°. Each crystallographically independent anion overlaps with its equivalence generated by symmetric transformation. A longitudinal and transverse offset was found in the dimer containing Ni(1) ions with the interatomic distances 4.032 Å of Ni(1)···Ni(1)^i and 3.482 Å of Ni(1)···S(4)^i (symmetric code i = $-x + 2, -y, -z + 1$), while the dimer consisting of Ni(2) ions with the interatomic distances 3.737 Å of Ni(2)···Ni(2)^j, 3.705 Å of S(5)···S(8)^j, and 3.634 Å of S(6)···S(7)^j (symmetric code j = $-x + 1, -y + 1, -z + 1$) was eclipsed. There are two types of dimer arrays, which are almost perpendicular to the direction of [1, −1, 0] as illustrated in Figure 2a. There are intermolecular interactions between stacks via S···S and S···Ni stacking interactions between them [the corresponding shorter interatomic contacts: 3.805 Å of S(1)···S(6), 3.811 Å of S(2)···S(7)^k, 3.771 Å of S(3)···S(6), 3.768 Å of S(3)···S(8), 3.809 Å of S(4)···S(7), and 3.601 Å of Ni(2)···S(2)^l; symmetric codes, k = $x + 1, y, z$; l = $x - 1, y, z$]. The H-bonding interactions between anions and cations were found as shown in Figure 2b, and geometric parameters are listed in Table 2. The adjacent anionic sheets are held together by cations through H-bonding interactions to develop into a 3D network.

The β phase crystallizes also in space group $P\bar{1}$ at 293 K, and the asymmetric unit consists of two $[Ni(mnt)_2]^-$ anions and one $[H_2DABCO]^{2+}$ cation in which the individual anionic and cationic structures are similar to those in the α phase. The significant differences concern the relative orientation between two crystallographically independent $[Ni(mnt)_2]^-$ anions and the patterns of H-bonding interaction (Figure 3). The dihedral angle between molecular planes (defined by NiS_4) of the two anions is 37.8°, which is much smaller than that in the α phase. An N−H proton in a cation interacts with three CN groups, as observed in the α phase. However, another N−H proton interacts with two CN groups to form bifurcated H-bonding interaction, which is distinct from the α phase. The anions are nearly eclipsed within two types of crystallographically independent dimers, which is elucidated by the shorter interatomic distances: 3.508 Å of Ni(1)···Ni(1)^i, 3.797 Å of Ni(1)···S(3)^i, 3.468 Å of S(1)···S(4)^i, 3.521 Å of S(2)···S(3)^i, 3.589 Å of Ni(2)···Ni(2)^j, 3.702 Å of Ni(2)···S(8)^j, 3.517 Å of S(5)···S(8)^j, and 3.572 Å of S(6)···S(7)^j (symmetric codes, i = $-x, -y + 2, -z$; j = $-x + 1, -y + 2, -z + 1$). Two types of dimers connect with their neighbors via S···S and Ni···S interactions into a sheet, as displayed in Figure 3a [the shorter interatomic contacts between neighboring dimers: 3.687 Å of S(2)···S(3)^k, 3.728 Å of S(3)···S(3)^l, 3.864 Å of S(3)···S(4)^m, 3.835 Å of S(3)···S(7)^n, 3.816 Å of S(5)···S(6)^m, 3.635 Å of S(6)···S(7)^k, 3.841 Å of S(7)···S(8)^m, 3.705 Å of S(8)···S(4)^p, and 3.461 Å of Ni(2)···S(4)^p; symmetric codes, k = $x - 1, y, z$; l =

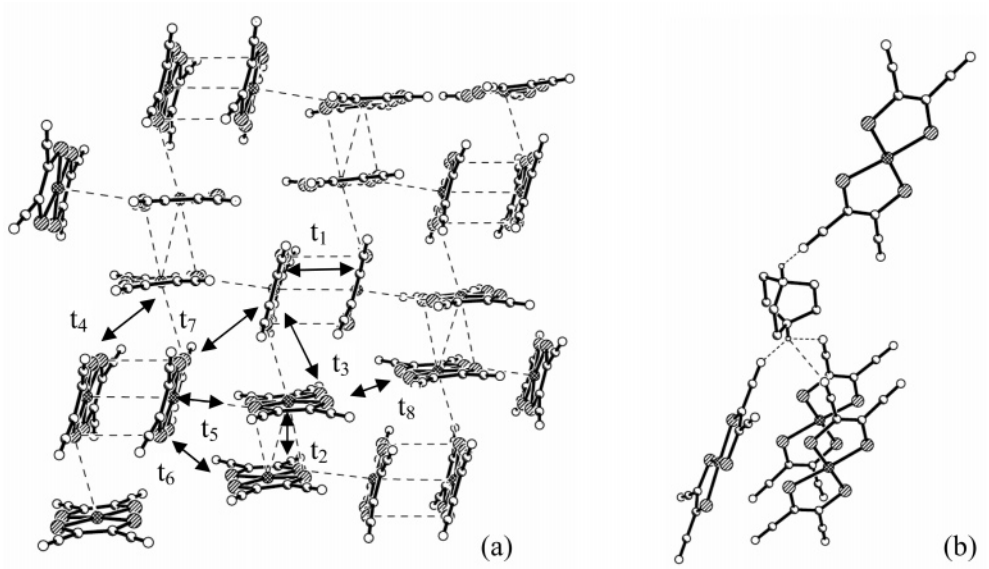

Figure 2. α phase: (a) 2D anionic layer showing two types of dimers with the schematic illustrations for magnetic-exchange paths; (b) scheme of H-bonding interaction between anions and cation.

Table 2. Parameters of H Bonds in the α and β Phases (Å and deg) at 293 K (100 K)

D−H···A	d(D−H)	d(H···A)	d(D···A)	∠(DHA)
		α Phase		
N(9)−H(9A)···N(3)#1	0.91 (0.91)	2.130 (2.153)	2.874 (2.879)	138.34 (136.16)
N(9)−H(9A)···N(8)#1	0.91 (0.91)	2.664 (2.574)	3.266 (3.182)	124.40 (124.81)
N(9)−H(9A)···N(5)#2	0.91 (0.91)	2.731 (2.621)	3.215 (3.124)	114.40 (115.67)
N(10)−H(10A)···N(7)#3	0.91 (0.91)	2.080 (2.060)	2.834(2.813)	139.59 (139.26)
symmetry transformations used to generate equivalent atoms:				
#1, $x, y+1, z-1$; #2, $-x+1, -y+2, -z$; #3, $-x, -y+1, -z+1$				
		β Phase		
N(9)−H(9A)···N(6)	0.91 (0.91)	2.354 (2.330)	2.989 (2.959)	126.79 (126.15)
N(9)−H(9A)···N(7)#1	0.91 (0.91)	2.490 (2.433)	3.058 (3.000)	120.82 (120.59)
N(9)−H(9A)···N(8)#2	0.91 (0.91)	2.251 (2.188)	2.905 (2.858)	128.39 (129.84)
N(10)−H(10A)···N(1)#3	0.91 (0.91)	2.693 (2.646)	3.214 (3.163)	117.33 (116.88)
N(10)−H(10A)···N(3)#4	0.91 (0.91)	2.002 (1.997)	2.784 (2.771)	143.04 (141.90)
symmetry transformations used to generate equivalent atoms:				
#1, $-x+1, -y+2, -z+1$; #2, $-x, -y+2, -z+1$; #3, $-x+1, -y+1, -z$; #4, $x, y-1, z$				

$-x+1, -y+2, -z$; m = $x+1, y, z$; n = $-x+1, -y+2, -z+1$; p = $-x, -y+2, -z+1$]. The H-bonding interactions between anions and cations link the adjacent anionic sheets into the 3D network.

The temperature dependences of paramagnetic susceptibility for two polymorphs were depicted in Figure 4. With regard to the α phase, the $\chi_m T$ value at 300 K is 0.34 emu·K·mol^{-1}, which approaches half of the spin-only value with two spins of $S = {}^1/_2$ per molecule. Upon cooling, the χ_m value rises gradually and reaches a maximum at around 120 K. The abrupt drop of the χ_m value below 120 K indicates a magnetic transition. A small hysteresis (∼1 K) was detected upon heating (Figure 4b). The χ_m value decreases exponentially below the magnetic transition to show the typical nature of a spin-gap system. The magnetic feature of the β phase is distinct from that of the α phase (Figure 4c) and shows the weaker paramagnetism in the overall temperature range. For example, the $\chi_m T$ value at 300 K is only 0.033 emu·K·mol^{-1}, which equals 4.3% of the spin-only value with two spins of $S = {}^1/_2$ per molecule. First, the susceptibility exponentially decreases and reaches a minimum at around 210 K and then increases again upon cooling. These attributes are representative of the ferrimagnetic behavior. A magnetic transition occurs at around 112 K with a hysteresis of ∼10 K upon heating. Below the transition, the magnetic susceptibility decreases again as the temperature is lowered.

The crystal structures in the low-temperature phase, as well as temperature-dependent cell parameters, were examined for the two polymorphs. As shown in Figure 5, the variation of the cell parameters with temperature is anisotropic. All α-phase cell parameters, except for the α angle and *a* axis, exhibit shortening upon cooling. The parameters *b* axis and α and β angles increase while others decrease upon cooling in the β phase. The intermolecular contacts, such as Ni···Ni, Ni···S, S···S, and N−H···N, as well as cell parameters vary gradually with cooling in two polymorphs, and the variation for each polymorph is less than 2% between the crystals at 293 and 100 K. These observations indicated that no structural transition was associated with the magnetic transition.

Further qualitative theoretical analysis for the magnetic-exchange interactions between the nearest spins was carried out within the tight-binding approximation for two poly-

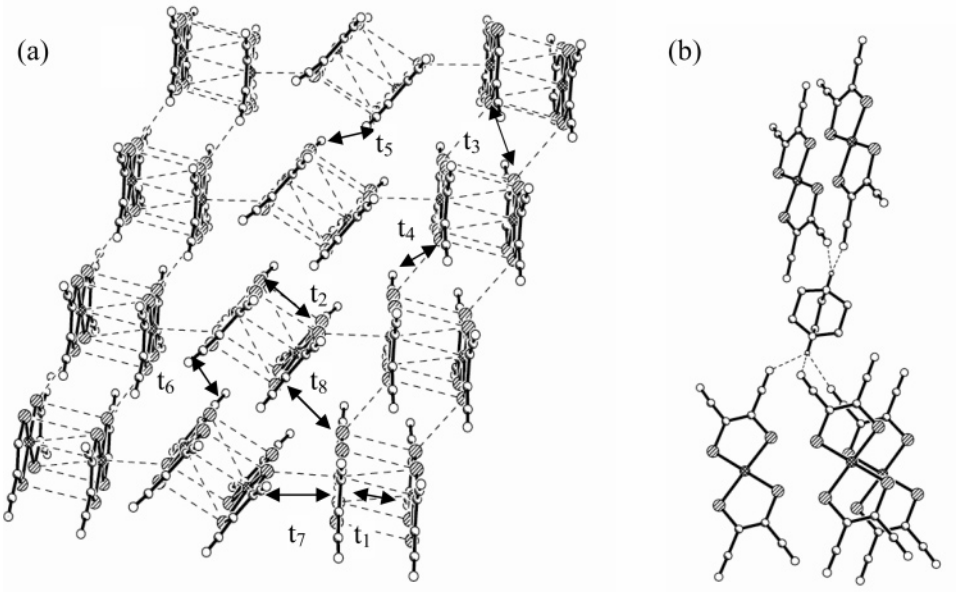

Figure 3. β phase: (a) 2D anionic layer showing two types of dimers with the schematic illustrations for magnetic-exchange paths; (b) scheme of H-bonding interaction between anions and cation.

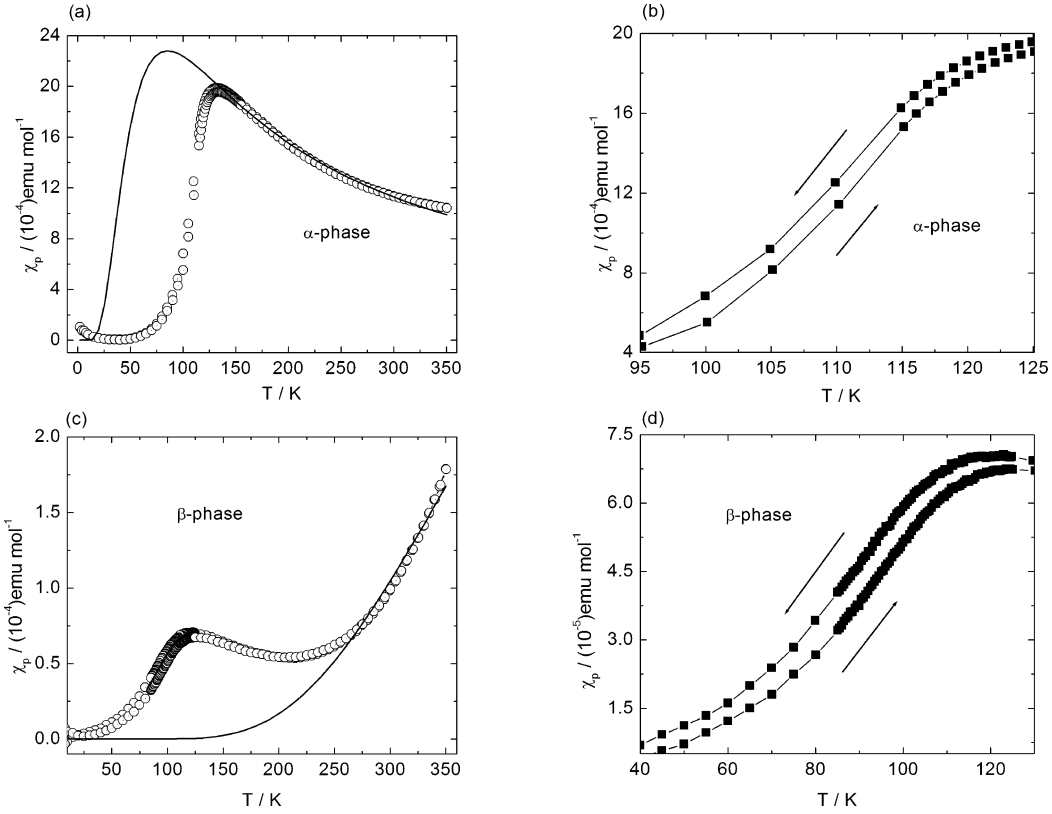

Figure 4. (a and c) Plots of magnetic susceptibility vs temperature for the α and β phases. The solid lines are reproduced from fitting parameters (referred to in the text) in the range of 130−350 K for the α phase and 260−350 K for the β phase. (b and d) Hysteresis loop for the α and β phases in which arrows indicate heating or cooling processes, respectively.

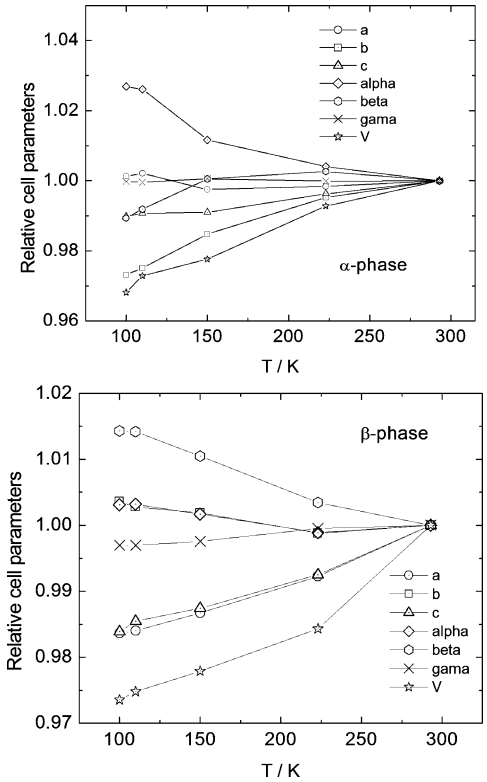

Figure 5. Relative cell parameters for both polymorphs, each of which is defined as $P(T)/P(293\ \mathrm{K})$, where $P(T)$ and $P(293\ \mathrm{K})$ represent the cell parameter at T and 293 K, respectively.

morphs at 293 and 100 K, using the extended Hückel molecular orbital calculation.[19] The singly occupied molecular orbitals of $[Ni(mnt)_2]^-$ anions and the published extended Hückel parameters for Slater-type atomic orbitals were utilized for calculations.[19b] In a spin system with Antiferromagnetic (AFM) interaction, the magnetic-exchange energy J_{AF} between two spin sites (spin dimer) is described as

$$J_{AF} \propto -(\Delta e)^2/U_{eff} \qquad (1)$$

where the magnetic−orbital interaction energy, Δe, is determined as the energy split between two magnetic orbitals in the spin dimer of $[Ni(mnt)_2]_2^{2-}$. U_{eff} is the effective on-site repulsive energy and is nearly constant for a defined magnetic solid. Therefore, J_{AF} is well approximated by the corresponding $(\Delta e)^2$.[20] Taking into account the magnetic-exchange interaction between the nearest neighbors, the spin dimers are schematically illustrated in Figures 2a and 3a for the α and β phases, respectively. The calculated results are presented in Table 3 and indicate the following: (1) In the α phase, the AFM interaction at 293 K is much stronger in the spin dimer of t_1 [corresponding to the crystallographic dimer of Ni(2)···Ni(2)^j ($j = -x + 1, -y + 1, -z + 1$)] than in others, and the magnetic-exchange interactions at 100 K in the spin dimers of t_1, t_3, t_4, and t_5 are comparable to those

(19) (a) Hoffmann, R. *J. Chem. Phys.* **1963**, *39*, 1397. (b) Dai, D.; Ren, J.; Liang, W.; Whangbo, M.-H. *CAESAR2 and SAMOA* (http://chvamw.chem.ncsu.edu).

(20) (a) Whangbo, M.-H.; Koo, H.-J.; Dai, D. *J. Solid State Chem.* **2003**, *176*, 417 and references cited therein. (b) Ribera, E.; Rovira, C.; Veciana, J.; Tarrés, J.; Canadell, E.; Rousseau, R.; Molins, E.; Mas, M.; Schoeffel, J. P.; Pouget, J.-P.; Morgado, J.; Gama, V.; Henriques, R. T.; Almeida, M. *Synth. Met.* **1999**, *102*, 1743.

Table 3. Values of $(\Delta e)^2$ [a] of Various Spin-Exchange Paths in a Layer for Both Polymorphs at 293 and 100 K, Where the Spin Dimers Are Identified by Specifying Their Ni···Ni Distances (Å)

	temperature			
	293 K		100 K	
spin dimer	Ni···Ni	$(\Delta e)^2$	Ni···Ni	$(\Delta e)^2$
		α Phase		
t_1	3.737	150233.8	3.697	172723.4
t_2	4.032	8742.3	4.113	50086.4
t_3	5.313	3069.2	5.202	2724.8
t_4	6.022	134.6	5.968	139.2
t_5	5.450	4719.7	5.416	4998.5
t_6	6.834	1.4	6.753	0.8
t_7	7.508	0	7.512	0
t_8	9.013	0	9.029	0
		β Phase		
t_1	3.590	205118.4	3.544	262451.3
t_2	3.508	305256.3	3.468	295174.9
t_3	6.478	8.4	6.372	28.1
t_4	6.918	2.9	6.833	0
t_5	6.477	0.8	6.372	1.0
t_6	6.874	10.2	6.838	4.8
t_7	5.078	29721.8	5.031	33819.2
t_8	6.411	204.5	6.208	750.8

[a] In units of meV^2.

at 293 K, whereas the magnetic-exchange interaction in the spin dimer of t_2 [corresponding to the crystallographic dimer of Ni(1)···Ni(1)^i ($i = -x + 2, -y, -z + 1$)] increases sharply, consistent with the changes of the stacking structures between 293 and 100 K (the distance of Ni···Ni shrinks in the spin dimers of t_1, t_3, t_4, and t_5, while it increases in the spin dimer of t_2). (2) In the β phase, the magnetic-exchange interaction for each spin dimer at 100 K is comparable to that at 293 K. The strongest exchange paths are found to concern two spin dimers, t_1 and t_2 [corresponding to the crystallographic dimers of Ni(1)···Ni(1)^i ($i = -x, -y + 2, -z$) and Ni(2)···Ni(2)^j ($j = -x + 1, -y + 2, -z + 1$), respectively], and the second-strongest exchange paths involve the spin dimer of t_7.

To combine the results of crystal structures and spin dimer analyses, it was found that the magnetic-exchange behavior of the α phase arises mainly from the entry containing the Ni(1) ion among two crystallographically independent anions due to the strong AFM interaction in the spin dimer, formed by two anionic entries containing Ni(2) ions. This leads to a diamagnetic ground state. This is potentially one of the reasons the $\chi_m T$ value at 300 K is near half of the spin-only value with two spins of $S = {}^1/_2$ per molecule. The very strong AFM interactions within two crystallographically independent anionic dimers are responsible for the weaker paramagnetism in the overall temperature range in the β phase. Thereby, the magnetic-exchange behavior of each polymorph in the high-temperature phase can be approximately described by a singlet−triplet model of an AFM-coupled $S = {}^1/_2$ dimer.

$$\chi_p = \frac{\chi_{dimer}}{[1 - (zJ'/Ng^2\beta^2)\chi_{dimer}]} \quad (2)$$

$$\chi_{dimer} = \frac{Ng^2{\mu_B}^2}{k_B T}[3 + \exp(-2J/k_B T)]^{-1} \quad (3)$$

where all symbols have their normal meanings. A reasonable fit to eq 2 was obtained with $J/k_B = -68.2$ K, $zJ'/k_B = -3.5$ K, and $g = 2.035$ for the α phase and $J/k_B = -680$ K, $zJ'/k_B = 2.2$ K, and $g = 2.012$ for the β phase. As for the compounds of $[Ni(mnt)_2]^-$, the magnetic-exchange feature is sensitive to the small changes in molecular overlap and interatomic contacts between $[Ni(mnt)_2]^-$ anions.[12b,21] Consequently, the temperature change, which affects interatomic contacts and overlapping patterns, switches a magnetic transition in two polymorphs.

Conclusions

In conclusion, a potential H-bonding donor cation, diprotonated 1,4-diazabicyclo[2.2.2]octane, was introduced into the magnetic system of $[Ni(mnt)_2]^-$ monoanion, and two polymorphs (α and β phases) were obtained that possess spin bistability. As expected, there exist H-bonding interactions between cations and anions and $\pi\cdots\pi$, S···S, and S···Ni interactions between anions. The strategy utilized to design new magnetic bistability molecular materials may be used for reference in the thriving field of functional molecular materials.

Acknowledgment. This work was partly supported by a Grant-in-Aid for Science Research from the Ministry of Education, Culture, Sports, Science and Technology of Japan. Authors thank Prof. Ichimura for use of the SQUID magnetometer. X.R. (JSPS fellow's ID No. P03271) thanks the Japan Society for the Promotion of Science for financial support.

Supporting Information Available: Crystallographic data of the α and β phases of **1** in CIF format and a figure of the temperature dependence of magnetization of the α and β phases. This material is available free of charge via the Internet at http://pubs.acs.org.

IC051563K

(21) Ni, Z. P.; Ren, X. M.; Ma, J.; Xie, J. L.; Ni, C. L.; Meng, Q. J. *J. Am. Chem. Soc.* **2005**, *127*, 14330.